shear bands can dramatically increase plasticity of BMGs (*32*). These results confirm that a structural feature is the cause of the super plasticity of the BMGs, and the homogeneous and concurrent formation of multiple shear bands throughout the samples is crucial for the improvement of plasticity in BMGs.

This unusual plasticity can shed light on some fundamental issues on the deformation and fracture of BMGs, such as the dynamics of plastic deformation (*5*). We measured the evolution of shear-band spacing d with increasing nominal strain ε. It was found that d correlates with ε via a power-law relation ($d = A\varepsilon^{-B}$) where A is a constant and $B = 1.45$, which is different from the value obtained by decreasing the sample's aspect ratio (height/diameter) to less than 1.0 (*8*).

Similar to the glass-forming ability of BMG-forming alloys (*33*), the super plasticity of the BMGs is very sensitive to their composition. Minor deviations in content (<1 atomic %) can substantially change the plasticity of the BMGs. The results indicate that, even in the reported BMG systems, extraordinarily plastic BMGs may be obtained by the appropriate choice of their composition with the use of the Poisson's ratio strategy. The present investigation has focused on Zr-based BMGs. We expect that the strategy would provide useful guidelines for the development of super plastic BMGs as high-performance structural materials in other known or unknown BMG-forming alloys and open an area of research of both fundamental and applied importance.

References and Notes

1. J. Schiøtz, K. W. Jacobsen, *Science* **301**, 1357 (2003).
2. K. S. Kumar, H. V. Swygenhoven, S. Suresh, *Acta Mater.* **51**, 5743 (2003).
3. A. L. Greer, *Science* **267**, 1947 (1995).
4. L. Q. Xing, Y. Li, K. T. Ramesh, J. Li, T. C. Hufnagel, *Phys. Rev. B* **64**, 180201 (2001).
5. D. M. Dimiduk, C. Woodward, R. LeSar, M. D. Uchic, *Science* **312**, 1188 (2006).
6. J. Das *et al.*, *Phys. Rev. Lett.* **94**, 205501 (2005).
7. Z. F. Zhang, H. Zhang, X. F. Pan, J. Das, J. Eckert, *Philos. Mag. Lett.* **85**, 513 (2005).
8. H. Bei, S. Xie, E. P. George, *Phys. Rev. Lett.* **96**, 105503 (2006).
9. J. Schroers, W. L. Johnson, *Phys. Rev. Lett.* **93**, 255506 (2004).
10. E. Ma, *Nat. Mater.* **2**, 7 (2003).
11. J. J. Lewandowski, W. H. Wang, A. L. Greer, *Philos. Mag. Lett.* **85**, 77 (2005).
12. Q. Zheng, H. Ma, E. Ma, J. Xu, *Scripta Mater.* **55**, 541 (2006).
13. X. J. Gu, A. G. McDermott, S. J. Poon, G. J. Shiflet, *Appl. Phys. Lett.* **88**, 211905 (2006).
14. W. H. Wang, *J. Appl. Phys.* **99**, 093506 (2006).
15. J. Lu, G. G. Ravichandran, W. L. Johnson, *Acta Mater.* **51**, 3429 (2003).
16. Y. Kawamura, A. Inoue, T. Masumoto, *Appl. Phys. Lett.* **71**, 779 (1997).
17. F. Spaepen, *Acta Mater.* **25**, 407 (1977).
18. T. El-Aguizy, J. S. Plante, A. H. Slocum, J. K. Vogan, *Rev. Sci. Instrum.* **76**, 075108 (2005).
19. M. N. Charalambides, S. M. Goh, L. Wanigasooriya, J. G. Williams, W. Xiao, *J. Mater. Sci.* **40**, 3375 (2005).
20. T. Mukai, T. G. Nieh, Y. Yoshihito, A. Inoue, K. Higashi, *Intermetallics* **10**, 1071 (2002).
21. T. C. Hufnagel, T. Jiao, Y. Li, K. T. Ramesh, *J. Mater. Res.* **17**, 1441 (2002).
22. W. J. Wright, R. Saha, W. D. Nix, *Mater. Trans.* **42**, 642 (2001).
23. J. Eckert *et al.*, *Intermetallics* **14**, 876 (2006).
24. C. Nagel, K. Rätzke, E. Schmidtke, F. Faupel, W. Ulfert, *Phys. Rev. B* **60**, 9212 (1999).
25. D. Suh, R. H. Dauskardt, P. A. Kumar, P. A. Sterne, R. H. Howell, *J. Mater. Res.* **18**, 2021 (2003).
26. T. Ichitsubo *et al.*, *Phys. Rev. Lett.* **95**, 245501 (2005).
27. A. S. Argon, *Acta Mater.* **27**, 47 (1979).
28. B. P. Kanungo, S. C. Glade, P. A. Kumar, K. M. Flores, *Intermetallics* **12**, 1073 (2004).
29. M. W. Chen, A. Inoue, W. Zhang, T. Sakurai, *Phys. Rev. Lett.* **96**, 245502 (2006).
30. L. M. Wang, W. H. Wang, R. J. Wang, *Appl. Phys. Lett.* **77**, 1147 (2000).
31. P. Murali, U. Ramamurty, *Acta Mater.* **53**, 1467 (2005).
32. Y. Zhang, W. H. Wang, A. L. Greer, *Nat. Mater.* **5**, 857 (2006).
33. D. Wang, H. Tan, Y. Li, *Acta Mater.* **53**, 2969 (2005).

34. Financial support is from the NSF of China (grant number 50621061) and the Chinese Academy of Sciences.

Supporting Online Material

www.sciencemag.org/cgi/content/full/315/5817/1385/DC1
Materials and Methods
Figs. S1 to S3
References

25 October 2006; accepted 4 January 2007
10.1126/science.1136726

Quantum Hall Effect in Polar Oxide Heterostructures

A. Tsukazaki,[1] A. Ohtomo,[1,2]* T. Kita,[3,4] Y. Ohno,[4] H. Ohno,[3,4] M. Kawasaki[1,5]*

We observed Shubnikov–de Haas oscillation and the quantum Hall effect in a high-mobility two-dimensional electron gas in polar ZnO/$Mg_xZn_{1-x}O$ heterostructures grown by laser molecular beam epitaxy. The electron density could be controlled in a range of 0.7×10^{12} to 3.7×10^{12} per square centimeter by tuning the magnesium content in the barriers and the growth polarity. From the temperature dependence of the oscillation amplitude, the effective mass of the two-dimensional electrons was derived as 0.32 ± 0.03 times the free electron mass. Demonstration of the quantum Hall effect in an oxide heterostructure presents the possibility of combining quantum Hall physics with the versatile functionality of metal oxides in complex heterostructures.

Zinc oxide (ZnO), a wide–band gap semiconductor, is of growing importance in advanced electronics, and its potential applications include transparent conducting oxide layers for flat-panel displays and transparent field-effect transistors (*1*). Research focused on the epitaxial growth of ZnO, particularly in terms of its novel excitonic properties, has led to the recent realization of homostructural light-emitting diodes (*2*). Studies of the intrinsic properties of ZnO have yielded a recipe for the preparation of high-quality epilayers having high mobility and excitonic luminescence with high quantum efficiency (*3*, *4*).

Certain aspects of two-dimensional electron gas (2DEG) behavior in semiconductor heterostructures have been studied by observing the quantum Hall effect (QHE)—a quantized magnetotransport accompanied by Shubnikov–de Haas (SdH) oscillations in the longitudinal resistivity ρ_{xx} and Landau plateaus in the Hall resistivity ρ_{xy} (*5*). Early results were obtained in the material systems of Si/SiO_2 or GaAs/AlGaAs (*6*, *7*). However, after discovery of the fractional QHE (*8*, *9*), the focus has been extended to a variety of other material systems, such as III-nitrides (*10*) and graphene (*11*). The observation of SdH oscillation requires conditions such as $\omega_c\tau > 1$ and $\hbar\omega_c > k_BT$, where ω_c is the cyclotron frequency equal to eB/m^* (where e is the charge on the electron, B is magnetic field, and m^* is the electron effective mass), τ is the carrier relaxation time, $\hbar$ is Planck's constant divided by 2π, k_B is Boltzmann's constant, and T is absolute temperature. Although several epitaxial oxide heterostructures have satisfied these conditions (*12*), the QHE has not been observed in those materials. [However, a QHE-like state was seen in a quasi-2D crystal of bulk η-Mo_4O_{14} (*13*).]

In our study, (0001)-oriented ZnO/$Mg_xZn_{1-x}O$ heterostructures were grown by laser molecular beam epitaxy with the use of a semiconductor-laser heating system (*3*). The $Mg_xZn_{1-x}O$ layer acts as a potential barrier for the 2DEG in the adjacent ZnO layer (*14*). We used a temperature gradient method that allowed us to grow the films over a wide range of temperatures on a single substrate (*3*). The three samples (samples A, B, and C) discussed here were of such high quality that we were able to look at the effects of growth temperature (T_g) of the ZnO layers and Mg content x in the barrier layers (Table 1) [see (*15*) for sample preparation and characterizations]. Sample A was selected from the highest-T_g region

[1]Institute for Materials Research, Tohoku University, Sendai 980-8577, Japan. [2]PRESTO, Japan Science and Technology Agency, Kawaguchi 332-0012, Japan. [3]ERATO Semiconductor Spintronics Project, Japan Science and Technology Agency, Sendai 980-0023, Japan. [4]Laboratory for Nanoelectronics and Spintronics, Research Institute of Electrical Communication, Tohoku University, Sendai 980-8577, Japan. [5]CREST, Japan Science and Technology Agency, Kawaguchi 332-0012, Japan.

*To whom correspondence should be addressed. E-mail: aohtomo@imr.tohoku.ac.jp (A.O.); kawasaki@imr.tohoku.ac.jp (M.K.)

of a film with an $x = 0.15$ barrier, whereas samples B and C were selected from lower- and intermediate-T_g regions, respectively, of another film with an $x = 0.2$ barrier. From the low-field Hall coefficient R_H, carrier densities $n = -1/(R_H e)$ and mobilities $\mu = -R_H/\rho_{xx}$ at 1 K were evaluated to be 0.66×10^{12} to 3.7×10^{12} cm^{-2} and 2700 to 5500 cm^2 V^{-1} s^{-1}, respectively. These values were nearly independent of temperature below 1 K, but with increasing temperature, n increased while μ decreased, eventually reaching the room-temperature values also listed in Table 1 (see fig. S4).

We found that n systematically depended on x and T_g for the ZnO layers. Our previous study showed that T_g was a good parameter to control the free carrier density; the intrinsic donor concentration increases with increasing T_g (*3*). To investigate the dependence on x, it is necessary to consider spontaneous and piezoelectric polarization effects along the polar (0001) orientation of wurtzite ZnO (*16*, *17*). These polarizations induce surface charges in individual layers, resulting in accumulation or depletion of free electrons at the heterointerfaces (*18*). Because the growth direction of our samples was identified to be the O-face (*2*), the direction of spontaneous polarization was upward toward the surface (Fig. 1A). From high-resolution x-ray diffraction analysis (fig. S3), the piezoelectric effect vanishes in unstrained $Mg_xZn_{1-x}O$ layers, whereas upward piezoelectric polarization should arise in ZnO layers from tensile strain (*14*). Thus, the total polarization is defined by

$$\sigma = [P_{sp}(0) + P_{pe}(x)] - P_{sp}(x) = |\Delta P_{sp}(x)| - |P_{pe}(x)| \quad (1)$$

where $P_{sp}(x)$ is spontaneous polarization in the $Mg_xZn_{1-x}O$ layer, and $P_{pe}(x)$ is piezoelectric polarization in the strained ZnO layer on unstrained $Mg_xZn_{1-x}O$. Note that positive σ means that free electrons are accumulated at the heterointerface, and negative σ means that free electrons are accumulated at the ZnO surface.

We calculated σ as a function of x (Fig. 1B). When x is higher than ~0.1, polarization-induced positive charges $|\sigma/e|$ (blue shading) are formed at the heterointerfaces, and their density increases as x increases. There is good agreement between experimental n (solid circles) and estimated $|\sigma/e|$, despite the ambiguity in $P_{pe}(x)$, a range of the theoretical values representing all of the shaded regions, and the lack of consideration of charge compensation with free electrons. Using the aforementioned polarization charges and band offset (*19*), we can construct the potential diagram near the heterointerfaces (Fig. 1C). The subband energies are estimated using a triangular-potential approximation (*20*) and are listed in the upper panel. The energy separations between the two lowest subband levels are greater than the Fermi energy, which suggests that in the temperature range of the experiments described below, carrier occupation in the second subband is negligible.

We measured the magnetotransport properties (Fig. 2, A and B) using a standard lock-in technique with ac excitation (10 nA, 19 Hz). At low field, all the samples exhibited negative magnetoresistance, presumably because of weakly localized carriers. Above ~ 2 T, clear ρ_{xx} oscillations that were periodic in $1/B$ appeared, and their amplitudes increased with increasing B. Although the zero-resistance state was absent because of the large scattering rate, each minimum of ρ_{xx} coincided with the quantized ρ_{xy} plateaus equal to $h/(\nu e^2)$, where ν is the Landau filling index. These observations confirmed the existence of the QHE in our samples and allowed direct determination of the 2DEG density (n_{2D}). Note that in sample A, the odd states, such as $\nu = 3$ and 5, had much wider Hall plateaus and larger amplitudes of ρ_{xx} minima relative to those of the even states (Fig. 2A). Consequently, the even states, such as $\nu = 4$, were barely observable in $d\rho_{xy}/dB$ (see circle superimposed on red broken line). These features were

Table 1. Growth and electronic parameters of $ZnO/Mg_xZn_{1-x}O$ heterostructures. Electron densities were obtained independently from the low-field Hall coefficient R_H and the low- and high-field slopes S_L and S_H, respectively (see Fig. 2C).

Sample	Thickness of ZnO (μm)	Growth temp. (°C)	Mg content x	Electron density (10^{12} cm^{-2})				Mobility μ (cm^2 V^{-1} s^{-1})	
				n_{2D}		$n = 1/R_H e$		R_H/ρ_{xx}	
				eS_L/h	eS_H/h				
				45 mK (A), 1 K (B, C)		1 K	300 K	1 K	300 K
A	1.1	1020	0.15	0.2	0.6	0.66	39	5500	150
B	0.4	900	0.20	0.4	1.2	1.8	5.0	4900	160
C	0.4	1000	0.20	0.9	1.8	3.7	11	2700	160

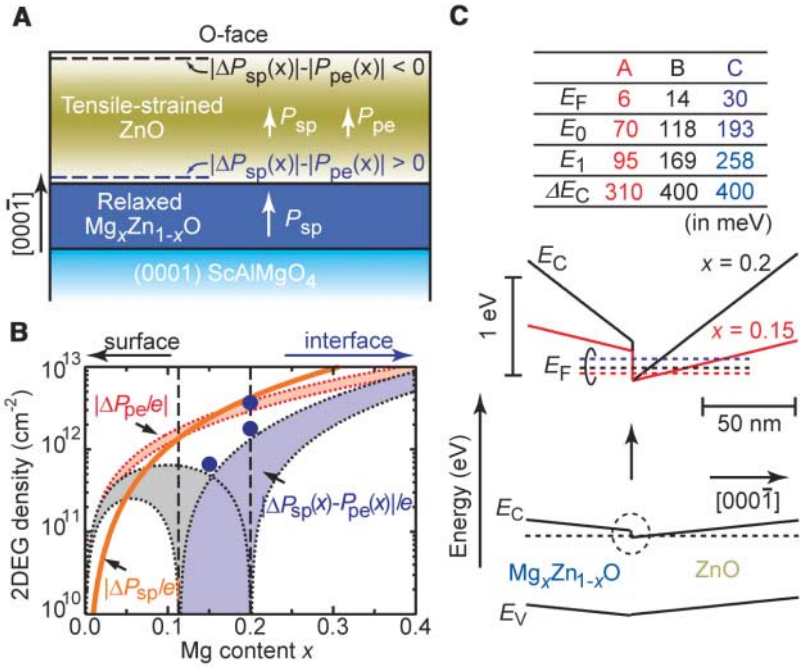

Fig. 1. (**A**) Schematic of the $ZnO/Mg_xZn_{1-x}O$ heterostructures grown on $ScAlMgO_4$ substrates. Depending on the sign of $|\Delta P_{sp}(x)| - |P_{pe}(x)|$, an accumulation layer represented by broken lines is formed either at the surface or in the interface. (**B**) Calculated (gray and blue shaded regions) and measured (solid circles) n as a function of Mg content x in the barrier. Red shaded region $[|P_{pe}(x)/e|]$ and solid orange curve $[|\Delta P_{sp}(x)/e|]$ were calculated by using theoretical values listed in tables S1 and S2. (**C**) Potential diagram near the heterointerfaces. Calculated energy parameters are listed in the upper panel, where E_F is the Fermi energy, E_0 and E_1 are the first and second subband energies with respect to the bottom of the conduction band in the wells, respectively, and ΔE_C is the conduction band offset. The colors of the potential profile (solid line) and position of E_F (broken lines) in the middle panel correspond to those of the upper panel, representing samples A, B, and C, respectively.

well preserved at elevated temperatures (see Fig. 2A and upper panel of Fig. 2D).

Standard analyses were performed using fan diagrams (Fig. 2C), where indices of extrema in ρ_{xx} and/or $d\rho_{xy}/dB$ are plotted as a function of $1/B$. Taking low- and high-field slopes (S_L and S_H), we independently evaluated n_{2D} as eS_L/h and eS_H/h, respectively, and compared these values with n (Table 1), where eS_H/h generally corresponds to the 2DEG density contributing to the QHE. The obtained eS_H/h values were systematically smaller than n by 9% to 51%, apparently indicating that 2D confinement becomes weaker with increasing n. To investigate carrier dimensionality, we further studied the B orientation dependence of the SdH effect under the configuration shown in the inset of Fig. 2D. Sample A exhibited weak oscillation, even with B parallel to the interface ($\theta = 90°$), and similar behavior was obtained for sample B (fig. S6). In contrast, sample C, which was expected to have more unconfined free carriers, showed vanishing oscillations with θ approaching 90°. The fact that the oscillation periods depended on the perpendicular B component $(B \cos \theta)^{-1}$, as evidenced by the data at $\theta = 30°$ (open circles in Fig. 2C), is consistent with a 2D character of the electron gas. In this regard, however, we found inconsistent results between n_{2D} extracted from fan diagrams and carrier dimensionality evidenced by angular dependencies of the SdH oscillations (see below).

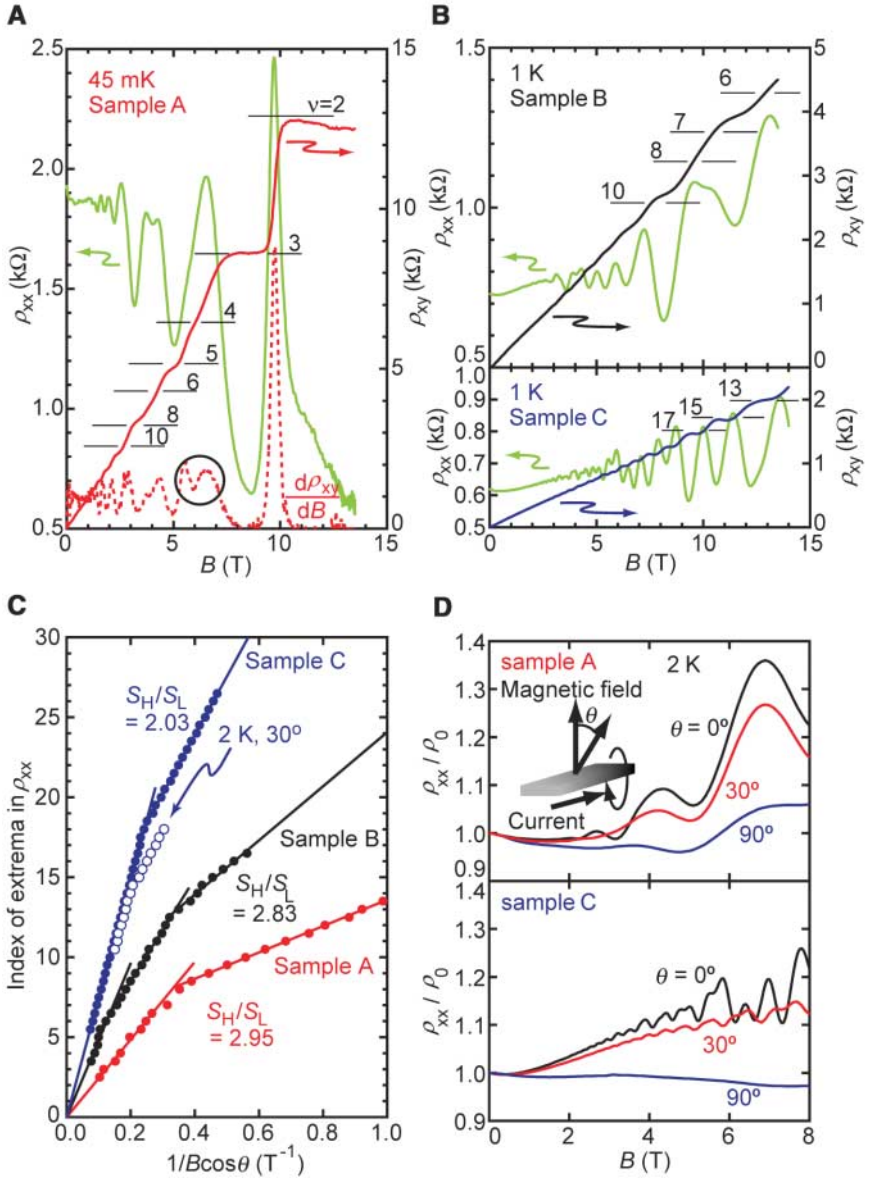

Fig. 2. (**A**) Longitudinal resistivity ρ_{xx}, Hall resistivity ρ_{xy}, and differential Hall resistivity $d\rho_{xy}/dB$ versus B measured at 45 mK for sample A. Integers on the horizontal tick marks are the Landau level filling factors defined as $\nu = h/(\rho_{xy}e^2)$. (**B**) ρ_{xx} and ρ_{xy} versus B measured at 1 K for samples B (top) and C (bottom). (**C**) Standard fan diagrams extracted from the data shown in (A) and (B). The symbols S_L and S_H refer to the low- and high-field slopes, respectively. Colors are consistent with those used for $\rho_{xy}(B)$ in (A) and (B). Open symbols were evaluated from data of sample C at 2 K and $\theta = 30°$ shown in (D). Note that each increment of index of extrema is set to 0.5. (**D**) Angular dependence of normalized magnetoresistance measured at 2 K for sample A (top) and sample C (bottom). Inset depicts the measurement configuration.

We next discuss anomalous periodicities of the SdH oscillations. The S_H/S_L ratios were found to be ~3 for samples A and B, and ~2 for sample C. These results suggest that an internal electric field arising from the asymmetric triangular well substantially removed spin degeneracy, even in zero magnetic field. In this case, the ratio of the slopes directly gives the carrier populations in two spin-split subbands, n_+ and n_-, as $S_H/S_L = 1 + n_+/n_-$. When applied to sample A, this analysis gives a carrier density in one band twice as large as that in the other band at low fields and total carrier density $n_{2D} = n_+ + n_- = 6 \times 10^{11}$ cm^{-2} (*25*, *26*). As for sample C, we obtained clear evidence of the 2D nature, and hence we expected that n_{2D} would be equal to n, but in fact we found that n_{2D} was about half of n. Together with the approximately linear slopes, this finding implies that the missed ρ_{xx} extrema occurred in a systematic fashion. In this situation, the values of n_{2D} and S_H/S_L are no longer reliable. Because of the stronger polarization fields in samples B and C, rather large spin splitting would be expected, making it difficult to resolve all Landau states (*23*). Relatively lower μ and higher ν may further reduce the ability to discriminate the Landau levels. In fact, even states with $\nu < 10$ tended to disappear in sample A, which has the highest μ. In the above discussion, we ignored the possibility of valley splitting because there was no evidence that either ZnO or $Mg_xZn_{1-x}O$ has an indirect band structure. Whether or not the spin-splitting scenario is likely in our samples, it is an interesting problem to be studied in future experiments.

Despite this open question, the observation of the $\nu = 2$ state is remarkable, particularly when compared with isostructural $Al_xGa_{1-x}N$/GaN heterostructures. It is difficult to obtain an n_{2D} value lower than 10^{12} cm^{-2} in nitrides having

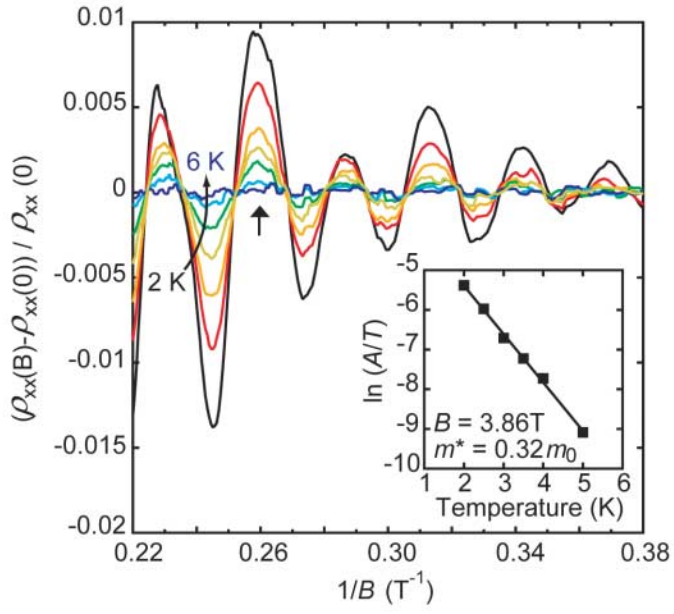

Fig. 3. Normalized magnetoresistivity versus 1/*B* recorded at various temperatures for sample C. Inset depicts temperature dependence of the logarithmic amplitude of ρ_{xx} peak at 3.86 T (indicated by arrow).

$Al_xGa_{1-x}N$ lattice constants smaller than GaN (*18*). A P_{pe} direction opposite to that in ZnO results in piling up of charges induced by both polarizations. Thus, our results imply the exciting possibility of realizing the fractional QHE in the present polar heterostructure if the carrier mobility can be improved. In addition, given chemical compatibility with certain other classes of oxides, the quantized Hall state may be combined with a broad range of physical properties in a complex oxide heterostructure.

References and Notes

1. K. Nomura *et al.*, *Science* **300**, 1269 (2003).
2. A. Tsukazaki *et al.*, *Nat. Mater.* **4**, 42 (2005).
3. A. Tsukazaki, A. Ohtomo, M. Kawasaki, *Appl. Phys. Lett.* **88**, 152106 (2006).
4. S. F. Chichibu *et al.*, *J. Appl. Phys.* **99**, 093505 (2006).
5. K. von Klitzing, G. Dorda, M. Pepper, *Phys. Rev. Lett.* **45**, 494 (1980).
6. J. Wakabayashi, S. Kawaji, *J. Phys. Soc. Jpn.* **44**, 1839 (1978).
7. D. C. Tsui, A. C. Gossard, *Appl. Phys. Lett.* **38**, 550 (1981).
8. D. C. Tsui, H. L. Stormer, A. C. Gossard, *Phys. Rev. Lett.* **48**, 1559 (1982).
9. R. Willett *et al.*, *Phys. Rev. Lett.* **59**, 1776 (1987).
10. M. A. Khan, J. N. Kuznia, J. M. Van Hove, N. Pan, J. Carter, *Appl. Phys. Lett.* **60**, 3027 (1992).
11. K. S. Novoselov *et al.*, *Science* **306**, 666 (2004).
12. A. Ohtomo, H. Y. Hwang, *Nature* **427**, 423 (2004).
13. M. Sasaki *et al.*, *Solid State Commun.* **109**, 357 (1999).
14. A. Ohtomo *et al.*, *Appl. Phys. Lett.* **72**, 2466 (1998).
15. See supporting material on *Science* Online.
16. I. B. Kobiakov, *Solid State Commun.* **35**, 305 (1980).
17. J. Jerphagnon, H. W. Newkirk, *Appl. Phys. Lett.* **18**, 245 (1971).
18. O. Ambacher *et al.*, *J. Appl. Phys.* **87**, 334 (2000).
19. A. Ohtomo *et al.*, *Appl. Phys. Lett.* **75**, 980 (1999).
20. F. Stern, *Phys. Rev. B* **5**, 4891 (1972).
21. R. J. Sladek, *Phys. Rev.* **110**, 817 (1958).
22. K. J. Button *et al.*, *Phys. Rev. Lett.* **28**, 1637 (1972).
23. T. Ando, A. B. Fowler, F. Stern, *Rev. Mod. Phys.* **54**, 437 (1982).
24. S. D. Sarma, *Phys. Rev. B* **27**, 2590 (1983).
25. H. L. Stormer *et al.*, *Phys. Rev. Lett.* **51**, 126 (1983).
26. J. P. Eisenstein, H. L. Stormer, V. Narayanamurti, A. C. Gossard, W. Wiegmann, *Phys. Rev. Lett.* **53**, 2579 (1984).

27. We thank S. F. Chichibu, K. Ueno, and T. Fukumura for valuable discussions. Supported by a Japan Society for the Promotion of Science research fellowship (A.T.); Creative Scientific Research grant 14GS0204 from the Ministry of Education, Culture, Sports, Science, and Technology of Japan; and the interuniversity cooperative program of the Institute for Materials Research, Japan.

Supporting Online Material

www.sciencemag.org/cgi/content/full/1137430/DC1
Materials and Methods
Figs. S1 to S6
Tables S1 and S2
References

10 November 2006; accepted 20 December 2006
Published online 25 January 2007;
10.1126/science.1137430
Include this information when citing this paper.

A Molecule Carrier

K. L. Wong,[1] G. Pawin,[1] K.-Y. Kwon,[1] X. Lin,[1] T. Jiao,[1] U. Solanki,[1] R. H. J. Fawcett,[1] L. Bartels,[1]* S. Stolbov,[2] T. S. Rahman[2]

We found that anthraquinone diffuses along a straight line across a flat, highly symmetric Cu(111) surface. It can also reversibly attach one or two CO_2 molecules as "cargo" and act as a "molecule carrier," thereby transforming the diffusive behavior of the CO_2 molecules from isotropic to linear. Density functional theory calculations indicated a substrate-mediated attraction of ~0.12 electron volt (eV). Scanning tunneling microscopy revealed individual steps of the molecular complex on its diffusion pathway, with increases of ~0.03 and ~0.02 eV in the diffusion barrier upon attachment of the first and second CO_2 molecule, respectively.

The development of molecules that, when adsorbed onto a surface, exhibit dynamic or electronic properties resembling those of macroscopic objects or machines has attracted considerable attention (*1*–*3*). Examples include rotors (*4*), nanocars and nanowalkers (*5*–*7*), various kinds of electrical switches and leads (*8*, *9*), and ratchets (*10*, *11*). For any realization of molecular-scale machinery, controlled transport of "cargo" molecules is a key functionality, much as transportation of macroscopic objects is the key purpose of many machines (e.g., conveyor belts, trucks). Control of surface transport by means of adsorbed molecules may additionally offer novel avenues for the optimization of surface processes such as growth/epitaxy, reactivity/catalysis, and friction/lubrication.

At metal surfaces, diffusion is generally the surface process with the lowest energetic barrier, hence it is the lowest-temperature surface process. Diffusion is random in nature and isotropic on flat surfaces unless the surface itself is anisotropic (*12*, *13*); step edges (*14*), anisotropic surfaces (*15*), and surface templates (*7*, *16*, *17*) can restrict diffusion to specific pathways or areas. The use of such surface features is, however, a very inflexible approach for guiding surface transport. Previous studies have shown that the isotropic diffusion of adsorbates on flat surfaces can be turned into linear and guided motion by means of incorporation of either two sequentially moving thiol substrate linkers (*6*) or fullerene "wheels" (*5*, *13*) into the adsorbate.

Although these approaches were successful for one specific molecule each, neither of them has yet been generalized to a class of molecules. Moreover, within the mentioned approaches, no transport of any "cargo" molecules has yet been realized, although concerted motion of adsorbates has been observed in unrelated systems (*18*, *19*). Here we show that anthraquinone (AQ) molecules (Fig. 1A) can transport one or two CO_2 molecules in a linear and guided fashion across an isotropic Cu(111) surface.

This study used a custom-built variable-temperature scanning tunneling microscopy (STM) system housed in a vacuum chamber

[1]Pierce Hall, University of California, Riverside, CA 92521, USA. [2]Department of Physics, University of Central Florida, Orlando, FL 32816, USA.

*To whom correspondence should be addressed. E-mail: ludwig.bartels@ucr.edu